Sensitivity of climate effects of hydrogen to leakage size, location, and chemical background

Ragnhild Bieltvedt Skeie[1], Marit Sandstad[1], Srinath Krishnan[1], Gunnar Myhre[1], and Maria Sand[1]

[1]CICERO Center for International Climate Research, Oslo, Norway

Correspondence to: Ragnhild Bieltvedt Skeie (r.b.skeie@cicero.oslo.no)

Abstract. Use of hydrogen can reduce carbon dioxide emissions by replacing fossil fuel used as an energy carrier and reactant in metal production. When hydrogen is used, some hydrogen will leak during production, storage, transport, and end use. Via ~~chemical~~OH-induced reactions in the atmosphere, the hydrogen will ~~affect the atmospheric composition of~~enhance methane, ozone, and stratospheric water vapor in the atmosphere and hence increase the radiation ~~in the atmosphere~~imbalance. A recent multi-model study found the Global Warming Potential over a 100-year time horizon (GWP100) for hydrogen to be 11.6 ±2.8 (one standard deviation). Here, we use a chemistry transport model to investigate the sensitivity of GWP100 to the magnitude and the location of the hydrogen emission ~~perturbation~~ and the chemical composition of the background atmosphere. We show that the hydrogen GWP100 is ~~linear with respect to~~independent of the size of the emission perturbation~~,~~; is not dependent on where emissions occur except sites far from soil sink active areas~~,~~; and is not very different for possible ~~futures of the~~future chemical compositions of the atmosphere. ~~We also investigate the~~For methane the CH$_4$ GWP100 ~~sensitivities on the atmospheric chemical composition, and it~~increases by up to 3.4 for different future atmospheric compositions compared to present-day~~atmospheric composition~~. Overall, the changes in the hydrogen GWP100 are within one standard deviation of the multi-model GWP100, except for emission perturbations at two distant sites not relevant for a future hydrogen economy. Therefore, ~~it is not necessary to adjust the multi-model GWP values~~ when assessing emissions at different locations or ~~in the~~for a future ~~where the~~with different atmospheric composition ~~differs from~~than present-day, it is not necessary to adjust the multi-model GWP values.

1 Introduction

In a low-carbon economy, molecular hydrogen ~~as an energy carrier~~ is expected to play a role as an energy carrier ~~(IEA, 2023;HydrogenCouncil, 2023;DNV, 2022).~~(IEA, 2023;HydrogenCouncil, 2023;DNV, 2022). Hydrogen is not a greenhouse gas and when it is used in a fuel cell to generate energy~~,~~. only water vapor is emitted. However, during production, storage, transport and end-use some hydrogen may leak (Esquivel-Elizondo et al., 2023). The leaked hydrogen will ~~chemically~~ react in the atmosphere with the hydroxyl radical (OH) and alter the ~~composition~~abundance of other greenhouse gases: methane (CH$_4$), ozone (O$_3$), and water vapor in the stratosphere (strat. H$_2$O) (Prather, 2003). The climate benefits of replacing fossil

30 fuel with hydrogen will depend on how much hydrogen is leaked, in addition to emissions related to the energy used to produce hydrogen (van Ruijven et al., 2011).

The climate effect of emissions of different gases can be compared using climate emission metrics (Forster et al., 2021). A commonly used metric is the Global Warming Potential (GWP). The GWP is defined as the ratio of the time integrated effective radiative forcing (ERF) over a given time horizon to a 1 kg pulse emission relative to that for 1 kg of CO_2. A time

35 horizon of 100 years is often used, GWP100. A shorter time horizon will give more weight to short-lived climate components (Fesenfeld et al., 2018;Shindell et al., 2017), such as H_2 with a lifetime of about 2 years (Ehhalt and Rohrer, 2009). A longer time horizon like 100 years, will give more weight ~~on~~to CO_2 and therefore be more appropriate for evaluating hydrogen as a replacement for CO_2 for reaching a long-term temperature stabilization target. The GWP100 is also used in an alternative method for evaluating the CO_2 mitigation potential GWP* (Cain et al., 2019;Allen et al., 2016) that

40 better ~~capture~~captures the temperature response of short- and long-lived greenhouse gases ~~named~~ (Allen et al., 2018;Lynch et al., 2020).

A H_2 GWP100 of 11.6 ± 2.8 was found in the multi-model study by Sand et al. (2023); 12 ± 6 using UK Earth System Model (UKESM1) chemistry–climate model (Warwick et al., 2023) and 12.8 ± 5.2 in Hauglustaine et al. (2022) based on GFDL-AM4.1 model results (Paulot et al., 2021). Studies that only include changes in the troposphere find smaller GWP100 values

45 (Derwent, 2023;Derwent et al., 2001;Field and Derwent, 2021;Derwent et al., 2020).

The largest source of uncertainty in the calculated GWP100 is the soil sink (Sand et al., 2023) and it is the largest - and most uncertain - term in the hydrogen budget (Ehhalt and Rohrer, 2009;Paulot et al., 2021). The soil sink varies geographically as it depends on the soil temperature and moisture as well as the biological activity (e.g. Paulot et al., 2021;Xiao et al., 2007). Due to ~~the land-ocean fraction~~greater landmass the soil sink is stronger in the Northern Hemisphere than in the Southern

50 Hemisphere. This results in ~~higher~~lower concentrations of hydrogen in the ~~Southern~~Northern Hemisphere, despite emissions dominating in the Northern Hemisphere. Using a two-dimensional tropospheric chemistry-transport model (TROPOS), Derwent (2023) studied the sensitivity of the H_2 GWP to the latitudinal dependence of the hydrogen emission pulse and found largest GWP values in the southernmost latitudes and weakest GWP values in the northernmost latitudes.

In addition to the soil sink, H_2 is removed from the atmosphere by chemical reaction with ~~the hydroxyl radical (OH).~~OH.

55 $$H_2 + OH \rightarrow H_2O + H \qquad (1)$$
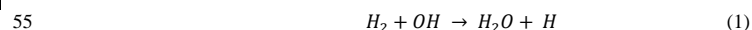
Photochemical reaction with OH is the ~~major~~dominant sink of methane, so when OH reacts with hydrogen (Eq.1) this will reduce the available OH for methane loss and therefore enhance the atmospheric lifetime of methane. The OH concentration is dependent on the methane levels and other components such as carbon monoxide (CO) and non-methane volatile organic

compounds (NMVOCs) that react with OH and hence reduce the OH levels. Nitrogen oxides (NO_x) on the other hand, ~~leads~~lead to photochemical production of OH in the atmosphere. The NO_x to CO emission ratio has been shown to be important for explaining the OH time evolution and changes in methane lifetime over time (Dalsøren et al., 2016;Skeie et al., 2023). The resulting H in Eq. 1 is involved in the complex photochemical ozone production. The ozone production is dependent on the concentrations of the ozone precursors ~~as~~ methane, CO, NMVOCs and NO_x in the atmosphere (Monks et al., 2015). Changes in atmospheric composition of these reactive gases influence the atmospheric lifetime of hydrogen and methane as well as the chemical production of ozone.

In this study we test the robustness of the GWP100 results presented in ~~the multi-model study by Sand et al. (2023), where GWP100 values were calculated based on steady-state simulations enhancing the hydrogen concentration globally by 10%.~~previous studies where hydrogen concentrations or hydrogen emissions are enhanced globally (Warwick et al., 2023;Hauglustaine et al., 2022;Sand et al., 2023). Here, we test the sensitivity to the geographical location of the hydrogen perturbation by adding 1 Tg yr^{-1} hydrogen emissions to seven different point locations using a three-dimensional atmospheric chemistry transport model. We also test the linearity of the calculated GWP100 (i.e. that the obtained GWP100 is independent of the size of the hydrogen emissions) by changing the magnitude of the emission perturbation in the model simulations. Finally, the atmospheric composition of ~~chemical~~chemically active species might be different in the future, which will influence the chemical loss of hydrogen through changes in OH concentrations as well as the chemical production of hydrogen in the atmosphere. Therefore, we investigate the sensitivity of the calculated GWP100 on the chemical composition of the atmosphere ~~on the calculated GWP100~~ using anthropogenic emissions and methane concentrations from three different Shared Socioeconomic Pathways (SSPs). In addition, based on the same model simulations, we calculate the CH_4 GWP100 and investigate how it differs for different chemical compositions of the atmosphere.

2 Methods

~~In this study we use the steady-state perturbation approach as in Sand et al. (2023) to calculate the GWP100 of hydrogen. We use the OsloCTM3, one of the models included in the multi-model study by Sand et al. (2023), to investigate the sensitivity of the calculated GWP100 due to the size and location of the hydrogen perturbation, as well as future atmospheric chemical compositions.~~

In this study we use an emission perturbation approach to calculate the GWP100 of hydrogen. We use the global chemical transport model OsloCTM3 to investigate the sensitivity of the calculated GWP100 due to the size and location of the hydrogen perturbation, as well as future atmospheric chemical composition.

2.1 GWP calculation

The H_2 GWP is the ratio of the absolute global warming potential (AGWP) for hydrogen relative to that for CO_2. The AGWP is defined as the time integrated effective radiative forcing of a 1 kg pulse emission over a given time horizon (Myhre et al., 2013). For a 100 year time horizon all the perturbations from an initial hydrogen pulse have decayed, and it is shown that a steady state perturbation matches the integrated response of a pulse emission (Prather, 2002;Prather, 2007).

To calculate the H_2 GWP100, a ~~set of three simulations were run to steady state: 1) a~~ control simulation~~, 2)~~ and a simulation with enhanced hydrogen emissions ~~and 3) a simulation with enhanced methane concentration~~are run to steady state. From the perturbed hydrogen simulation, the change in atmospheric composition of O_3, CH_4, and strat. H_2O and the resulting ERFs due to these changes are calculated. ~~Because the~~ As emission driven simulations of methane are challenging due to large uncertainties in the methane sources and sinks (Saunois et al., 2020), global chemical models fix the surface concentration of methane. The change in the atmospheric methane is ~~fixed at the surface,~~ calculated from the modeled change in methane lifetime. As changes in methane also change the composition of O_3 and strat. H_2O a methane perturbation experiment is also needed ~~to take into account~~. From the methane perturbation experiment, where hydrogen is the same as in the control simulation, the atmospheric composition changes of O_3 and strat. H_2O, and hence the ERF, due to the changes in the methane lifetime in the hydrogen perturbation experiment can be extracted. The contributions to the H_2 GWP100 from the changes in the methane lifetime are referred to as "methane induced". From the methane perturbation experiments performed, we also calculate the CH_4 GWP100.

We follow the same approach as in the multi-model study by Sand et al. (2023). While the hydrogen concentration was perturbed in the main simulations in that study, we use hydrogen emission perturbations and investigate the sensitivity of the GWP100 to how the perturbations are implemented in the model.

~~From the methane perturbation experiments performed, we also calculate the CH_4 GWP100.~~

2.2 Sensitivity experiments

Three sets of sensitivity tests are performed. In the first set of sensitivity tests, we test if the ~~linearity of~~calculated GWP100 is dependent on the size of the emission perturbation ~~on the calculated GWP100.~~. The anthropogenic emissions of hydrogen are scaled so that the global emissions increase by 0.1, 1, 10 and 100 Tg yr^{-1} (anthro01, anthro1, anthro10 and anthro100).

The second set of sensitivity tests investigate the dependence on the geographical location of the perturbations. Point source ~~emission~~emissions of 1 Tg yr^{-1} are added to seven locations (Fig. 1) expected to span a wide range of possible model responses. As the soil sink is only active over land, we choose point emissions over the point furthest from land (nemo) located in the South Pacific; the most landlocked point (epia); ~~the point with the highest soil sink reported by the model in East Africa close to the Equator (maxdep); a point in~~ a point in the US in an area with large soil sink velocities in the model

(usdrydep); a point in East Africa close to the Equator where the soil sink velocity is large (lowlatdep); a more typical industrial point over Europe (munich); in addition to an Arctic (zep); and an Antarctic (maud) point (Table 1). The sites are indicated by stars in Fig. 1.

120   For these first 11two sets of sensitivity tests, the same methane perturbation simulation enhancing 2010 methane surface concentration by 10%, similar to Sand et al. (2023) was used to gauge the methane induced changes (Table 2). Note that the methane perturbation and the sensitivity tests for hydrogen perturbations correspond to two different control simulations, as hydrogen is concentration driven in the methane perturbation simulation. and emission driven in the hydrogen perturbation simulations.

125   The last set of sensitivity tests investigate the sensitivity of the calculated GWP100 onto the atmospheric composition. We use the same setup as for the other simulations but use methane surface concentration (Meinshausen et al., 2020) and gridded anthropogenic emissions for 2050 from three different SSPs (Gidden et al., 2019): SSP119, SSP434 and SSP585. The SSPs chosen were based on high and low methane concentration (Fig. 2a) and high and low NO_x to CO emission ratio (Fig. 2b) as it is found to be a main driver of change in OH and methane lifetime (Dalsøren et al., 2016;Skeie et al., 2023) and would also

130   influence the atmospheric lifetime of hydrogen. For each SSP, a control simulation, a 10 Tg yr^{-1} hydrogen emission increase simulation (as anthro10) (Table 1) and a 10% increase in surface methane concentration (Table 2) simulation are performed.

2.3 Model description

The OsloCTM3 (Søvde et al., 2012) is a chemistry transport model driven by 3-hourly meteorological forecast data generated by the Open Integrated Forecast System (OpenIFS, cycle 38 revision 1) at the European Centre for Medium-Range

135   Weather Forecasts (ECMWF), and the horizontal resolution is ~2.25 × 2.25° with 60 vertical layers ranging from the surface and up to 0.1 hPa. The OsloCTM3_ model is used in a similar set up as in Sand et al. (2023), except that the calculation of stratospheric water vapor has been updated to ensure a balanced hydrogen budget in the stratosphere and the implementation of the geographical distribution of the anthropogenic emissions of hydrogen that was shifted 180 degrees has been corrected. The hydrogen soil sink scheme takes into account the soil moisture effect on dry-deposition velocities that depend on

140   vegetation types (Sanderson et al., 2003) with no uptake for snow covered land and reduced uptake rate for cold surfaces (Price et al., 2007). For the sensitivity test with present-day atmospheric composition, the anthropogenic emissions used are from the Community Emissions Data System (CEDS) (version 2017-05-18) (Hoesly et al., 2018), biomass burning emissions from Global Fire Emissions Database (van der Werf et al., 2017) and the hydrogen emissions from Paulot et al. (2021). Emissions for the year 2010 were used from all three datasets. For the sensitivity tests with different atmospheric

145   backgrounds, the anthropogenic emissions used are 2050 emissions from the three SSP scenarios (Gidden et al. (2019), SSP119: IAMC-IMAGE-ssp119-1-1, SSP434: IAMC-GCAM4-ssp434-1-1, SSP585: IAMC-REMIND-MAGPIE-ssp585-1-1), while hydrogen emissions and biomass burning emissions are kept the same as for the present-day simulations. The

model is run with 2009 and 2010 meteorology repeatedly for in total 26 years, except for the methane concentration perturbations that were run for 20 years.

2.4 Forcing calculation

The forcing components included in the GWP100 calculations are CH_4, O_3 and strat. H_2O. ~~As in Sand et al. (2023) the~~The ERFs for these components are calculated from the last year of the OsloCTM3 steady-state simulations. The CH_4 ERF is calculated using a concentration-to-forcing factor of 0.448 mW m^{-2} ppb^{-1} (Etminan et al., 2016) with an adjustment term of -14% (Forster et al., 2021)~~.~~, where the adjustment term converts the forcing from stratospheric temperature adjusted radiative forcing to ERF. The ERF of O_3 is calculated using monthly mean three-dimensional O_3 fields in the perturbations compared to the control simulation multiplied by a monthly three-dimensional kernel for O_3 radiative forcing (RF) that includes stratospheric temperature adjustments (Skeie et al., 2020). No tropospheric adjustments are assumed, and the resulting radiative forcing values are treated as ERF. For strat. H_2O, the RF values calculated offline using radiative transfer schemes for longwave and shortwave radiation separately (Myhre et al., 2007) are also treated as ERF, assuming no tropospheric adjustments.

Table 1: List of sensitivity tests for the hydrogen emission perturbation. In the sensitivity tests, the anthropogenic hydrogen emissions (anthro) are perturbed. Each of the SSP-sensitivity tests have separate corresponding control simulations, while the tests with different magnitude of the emission ~~perturbation~~perturbations and the tests with different geographical point emission perturbations share the same control simulation.

Name of sensitivity test	Description of test
anthro01	anthro+0.1 Tg yr^{-1}
anthro1	anthro+1 Tg yr^{-1}
anthro10	anthro+10 Tg yr^{-1}
anthro100	anthro+100 Tg yr^{-1}
epia	anthro+1Tg yr^{-1} in the middle of the continents (46.17 N, 85.58 E)
maud	anthro+1Tg yr^{-1} in Antarctica (72.3 S, 12 E)
~~maxdep~~lowlatdep	anthro+1Tg yr^{-1} where model soil sink is largest (3.3 N, 41.0E)
munich	anthro+1Tg yr^{-1} in central Europe (48.1 N, 11.6 E)
nemo	anthro+1Tg yr^{-1} in the middle of the ocean (48.5 S, 123.2 W)
usdrydep	anthro+1Tg yr^{-1} in US where soil sink is large (34.8 N,100.7 W)
zep	anthro+1Tg yr^{-1} in the Arctic (78.5 N, 11.56 E)
SSP119	anthro+10 Tg yr^{-1} in 2050 SSP1-1.9 chemical atmosphere

| SSP434 | anthro+10 Tg yr⁻¹ in 2050 SSP4-3.4 chemical atmosphere |
| SSP585 | anthro+10 Tg yr⁻¹ in 2050 SSP5-8.5 chemical atmosphere |

Table 2: List of methane sensitivity ~~test. The surface concentration of methane in the control simulation is given in parenthesis~~tests. The Present-day sensitivity test is used for all size and location perturbations, while each SSP test has a corresponding SSP methane sensitivity test.

Name of sensitivity test	Description of test
Present-day	10% increase in surface concentration ~~(~~from 1813 ppbv~~)~~ in the control
SSP119	10% increase in surface concentration ~~(~~from 1427 ppbv~~)~~ in the control
SSP434	10% increase in surface concentration ~~(~~from 2223 ppbv~~)~~ in the control
SSP585	10% increase in surface concentration ~~(~~from 2446 ppbv~~)~~ in the control

170

a) Annual Anthropogenic H_2 emissions [mg m^{-2} yr^{-1}]
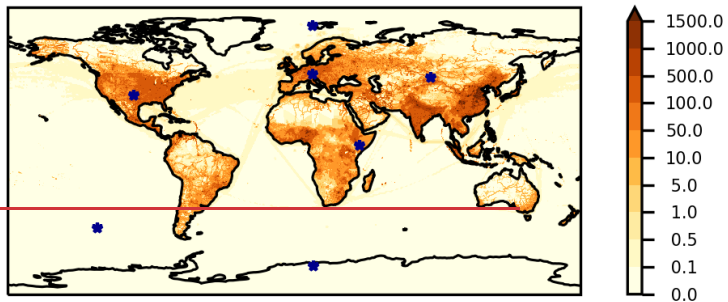
b) Annual Soil Sink H_2 [mg m^{-2} yr^{-1}]
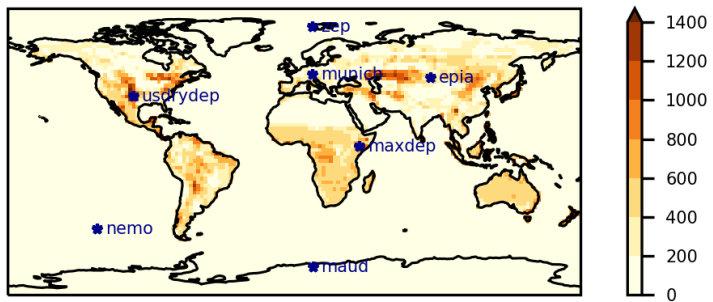
a) Annual Anthropogenic H$_2$ emissions [mg m^{-2} yr^{-1}]
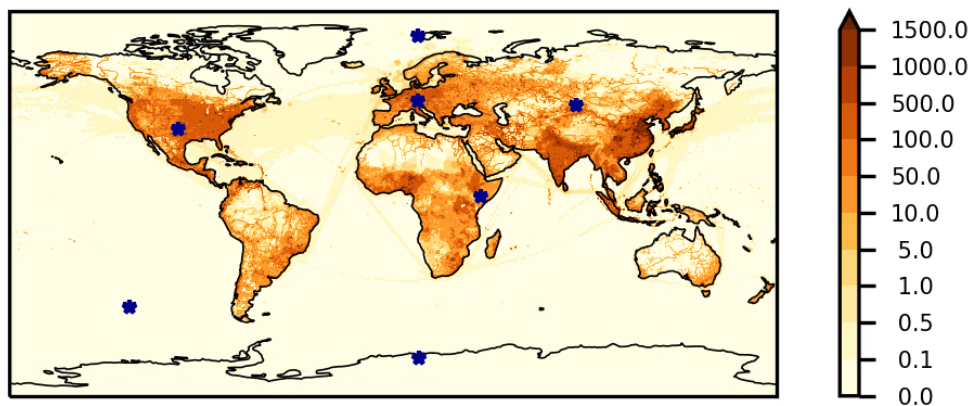
b) Annual H$_2$ deposition velocity [cm s^{-1}]
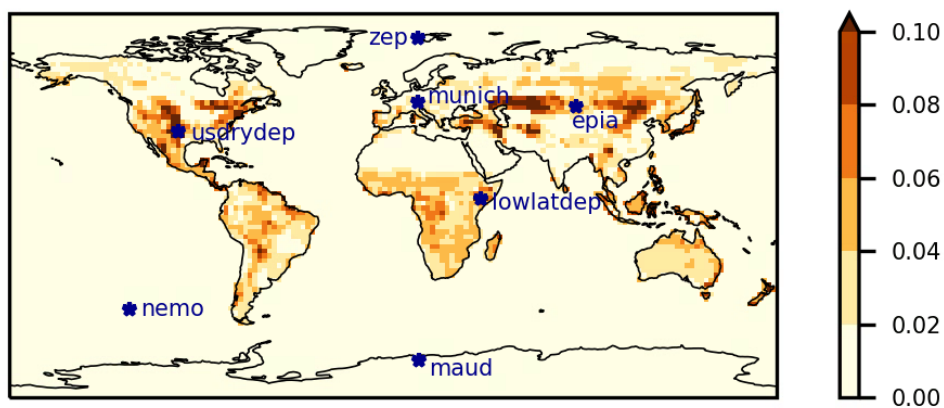
Figure 1: In a) the total annual anthropogenic emissions of hydrogen from Paulot et al. (2021) for 2010 is shown and in b) the ~~total~~ annual ~~soil sink~~mean deposition velocity of hydrogen from OsloCTM3 ~~from the~~ present-day control simulation is shown. In both figures, the sites where 1 Tg yr^{-1} is added in the sensitivity tests for perturbation locations ~~is~~are indicated by a blue star and in b) the names of the respective sensitivity tests are also indicated.
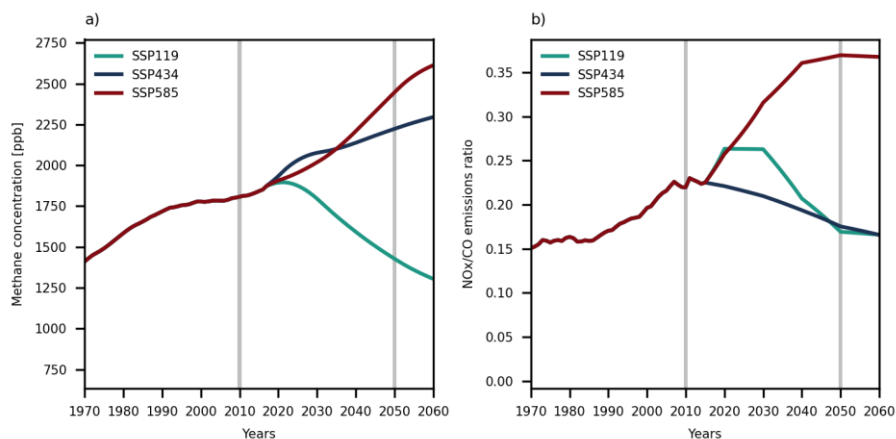
Figure 2: In a) the historical and future methane surface concentrations and in b) the historical and future anthropogenic NOₓ to CO emission ratios. The three SSPs used in this study are shown. The years used in the simulations (2010 and 2050) are indicated by a vertical line. The anthropogenic emissions for NOₓ and CO separately, in addition to volatile organic components (VOCs) are shown in Fig. S1.

3 Results

The resulting H_2 GWP100 values from all the sensitivity tests are shown in Fig. 3. The individual contributions from methane are in green; ozone in yellow; and stratospheric water vapor in purple. The hashed areas show how much of the change is due to changes in methane lifetime. Also added to the figure is the multi-model H_2 GWP100 from Sand et al. (2023) where the uncertainty bar indicates one standard deviation uncertainty range based on spread in underlying values found in literature and from the model ensemble. ~~The individual contributions from methane are in green; ozone in yellow; and stratospheric water vapor in purple. The hashed areas show how much of the change is due to changes in methane lifetime.~~

3.1 ~~Are~~Is the ~~results~~response to emissions size linear?

The first set of sensitivity tests investigate the linearity in the ~~results~~chemical response with respect to the magnitude of the hydrogen emission perturbation. Adding a hydrogen perturbation of 0.1, 1, 10 or 100 Tg yr⁻¹ resulted in very similar GWP100 values ranging from 12.2 to 12.6 as seen in the first 4 bars in Fig. 3. To conclude, the GWP100 values are ~~linear with respect to~~independent of the magnitude of the emission perturbation~~.~~ within the range 0.1 to 100 Tg yr⁻¹
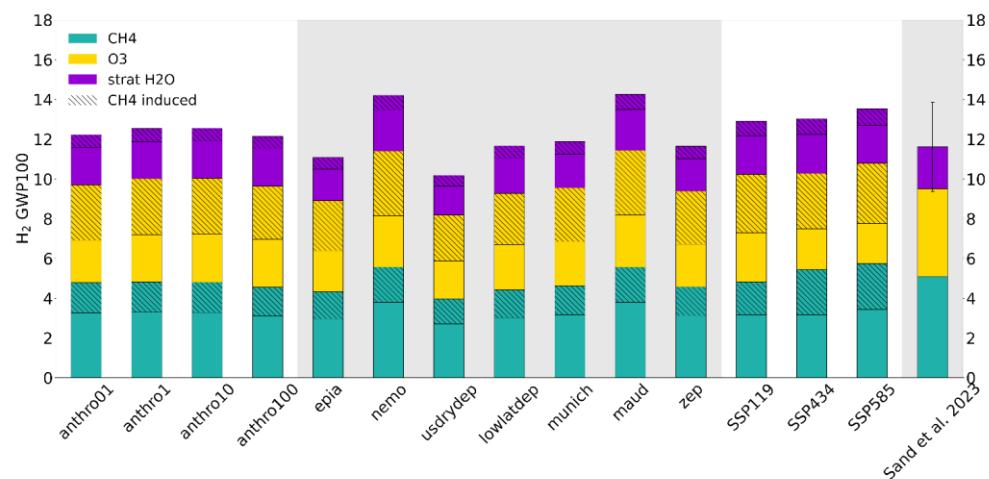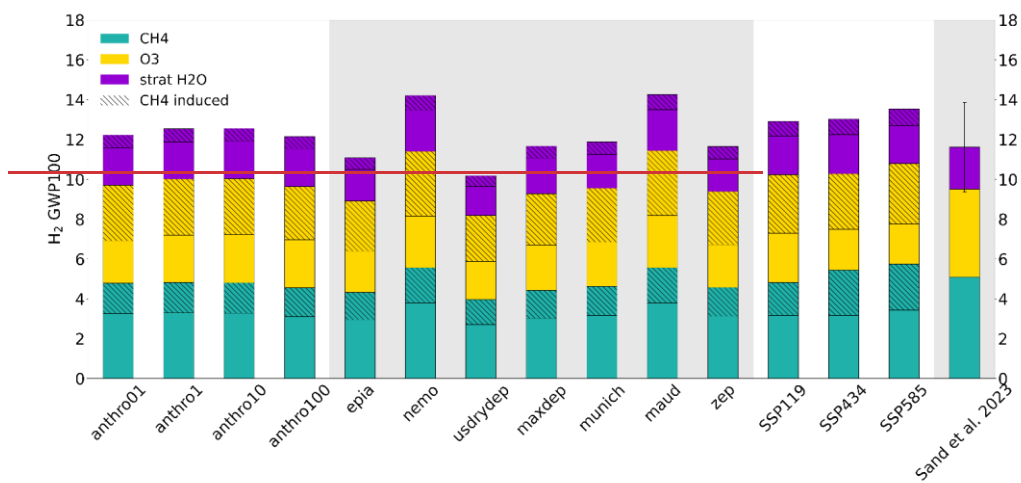
Figure 3: The H₂ GWP100 for the different sensitivity tests (Table 1) where the individual contributions from methane (green), ozone (yellow), and stratospheric water vapor (purple) as well as methane induced changes in these (hashed) are shown. The multi model mean with uncertainty range (one standard deviation) assessed in Sand et al. (2023) is shown to the right. The GWP100 values are presented in Table S1.

200

205

3.2 Does location matter?

The second set of sensitivity tests investigate the GWP100 sensitivity to the geographical location of the hydrogen emission perturbation. In anthro1, 1 Tg yr^{-1} was added in the simulation by scaling the anthropogenic emissions while in these simulations, 1 Tg yr^{-1} is added in seven specific point locations around the globe (Table 1). The point locations are carefully

210   selected to span a wide range of possible GWP values based on distance to soil sink active areas and latitude (Fig. 1b). The resulting GWP100 values range from 10.2 to 14.2 (Table S1), which is 19% lower and 14% higher than the anthro1 GWP100 of 12.5 (Fig. S2).

Figure 4a shows the increase in global mean surface hydrogen concentration per hydrogen flux for all sensitivity simulations. The hydrogen surface concentrations are highly dependent on where the hydrogen perturbation is added in the simulation

215   (bars on grey background in Fig. 4a). Adding 1 Tg H$_2$ yr^{-1} at the ocean site (nemo) and in Antarctica (maud) results in larger increases in hydrogen concentrations of 7.9 and 9.2 ppb than adding the 1 Tg H$_2$ yr^{-1} to areas with large soil sink in the model such as usdrydep and maxdeplowlatdep, which hasshow an increase of 5.2 and 5.4 ppb respectively (Fig. 1b). The more typical industrial area (munich) has a very similar change in atmospheric hydrogen per flux of hydrogen compared to the anthro1 simulation, both with 6.3 ppb per 1 Tg H$_2$ yr^{-1}.

220
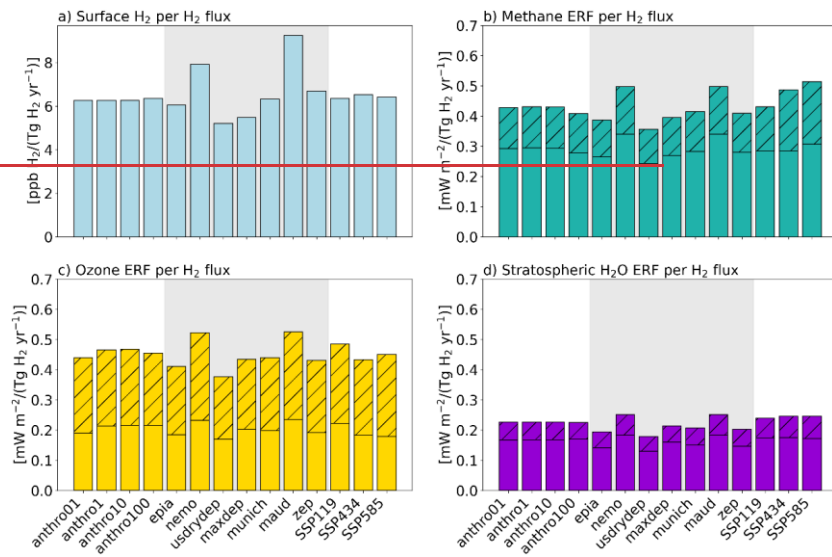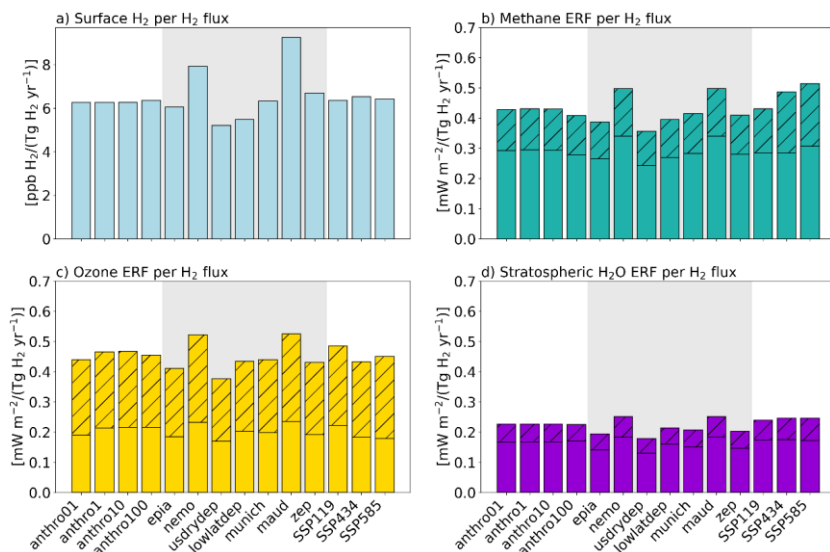
Figure 4: Changes in a) surface hydrogen concentration, b) ERF of methane, c) ERF of ozone and d) ERF of stratospheric water vapor due to 1 Tg yr^{-1} flux of hydrogen. The methane induced changes are indicated by the hatching. The underlying numbers for these figures are presented in ~~Table~~Tables S2-S4.

The difference in the increase of atmospheric hydrogen concentration per flux of hydrogen can be explained by ~~the feedback factor. The feedback factor is the lifetime of the perturbation divided by the lifetime of the atmospheric component. For chemical~~different perturbation lifetimes. For chemically reactive species, such as methane, the chemical loss in the atmosphere via OH will be less efficient when more methane is added to the atmosphere, and the lifetime of the methane perturbation is enhanced. For methane the chemical feedback factor (the lifetime of the perturbation divided by the background lifetime of the atmospheric component) is larger than 1 (Holmes et al., 2013;Sand et al., 2023;Thornhill et al., 2020)~~. For the ocean site (nemo) and Antarctic site (maud), the hydrogen feedback factor is larger than 1 (Table 3). These are areas far away from soil sink active areas, and the removal via OH which are then dominating, is less efficient when more hydrogen is added, hence the feedback factor is larger than 1.~~

~~For the other sites, as well as when global anthropogenic emissions are perturbed (anthro simulations), the hydrogen feedback factor is less than 1.~~. For a hydrogen perturbation, the geographical distribution of the emission perturbation influences the perturbation lifetime (Table 3). For the atmospheric lifetime, the perturbation lifetime is larger than the lifetime, with the largest increase of 10% at the Antarctic site (maud). For the soil sink lifetime, the perturbation lifetime is

shorter than the hydrogen background lifetime except for the ocean site (nemo) and Antarctic site (maud) (Table 3). The soil sink is enhanced when emissions are close to the soil sink active areas relative to the total soil sink~~, and therefore the feedback factor is less than 1. The lowest feedback factor is for usdrydep with 0.76~~ and hence the perturbation lifetime is reduced. As the soil sink lifetime (3.5 years) is lower than the atmospheric lifetime (7.0 years) a similar change is seen for the total perturbation lifetime relative to total background lifetime as for the soil sink lifetime (Table 3). The largest difference between the perturbation lifetime and the hydrogen lifetime is for usdrydep with a difference of 0.57 years.

Table 3: Total lifetime of hydrogen (total burden divided by the total loss in the control simulation), ~~feedback factor and perturbation lifetimes in the different sensitivity tests~~**atmospheric lifetime (total burden divided by the atmospheric loss in the control simulation) and soil sink lifetime (total burden divided by the soil sink loss) and the respective perturbation lifetimes (change in burden divided by change in loss in the perturbation simulation relative to the control simulation) for the different sensitivity tests. The change in perturbation lifetime relative to the lifetime in the control simulation (in %) are given in the parentheses.**

	H₂ total lifetime [yrs]	~~Feedback factor~~ H₂ perturbation lifetime [yrs]	H₂ atmospheric lifetime [yrs]	H₂ atmospheric perturbation lifetime [yrs]	H₂ soil sink lifetime [yrs]	H₂ soil sink perturbation lifetime [yrs]
anthro01	2.35	~~0.92~~ 2.17 (-7.5)	7.02	7.23 (3.1)	3.53	3.10 (-12)
anthro1	2.35	~~0.92~~ 2.17 (-7.5)	7.02	7.24 (3.2)	3.53	3.10 (-12)
anthro10	2.35	~~0.93~~ 2.17 (-7.4)	7.02	7.27 (3.6)	3.53	3.10 (-12)
anthro100	2.35	~~0.94~~ 2.20 (-6.3)	7.02	7.55 (7.6)	3.53	3.10 (-12)
nemo	2.35	~~1.09~~ 2.56 (9.0)	7.02	7.64 (8.9)	3.53	3.85 (9)
epia	2.35	~~0.83~~ 1.94 (-17.2)	7.02	7.25 (3.3)	3.53	2.66 (-25)
munich	2.35	~~0.89~~ 2.08 (-11.3)	7.02	7.24 (3.2)	3.53	2.92 (-17)
usdrydep	2.35	~~0.76~~ 1.77 (-24.5)	7.02	7.18 (2.3)	3.53	2.35 (-33)
maud	2.35	~~1.10~~ 2.59 (10.2)	7.02	7.73 (10.2)	3.53	3.89 (10)
zep	2.35	~~0.89~~ 2.09 (-11.0)	7.02	7.40 (5.5)	3.53	2.91 (-17)
~~maxdepl~~ owlatdep	2.35	~~0.85~~ 1.99 (-15.0)	7.02	7.22 (2.9)	3.53	2.75 (-22)
SSP119	2.37 ~~0.94~~ 2.20	2.22 (-6.9)	7.26	7.59 (4.6)	3.51	3.11 (-12)
SSP434	2.45 ~~0.93~~ 2.26	2.28 (-7.8)	7.95	8.26 (3.9)	3.54	3.11 (-12)

| SSP585 | 2.41 | 2.22 8.0.9 (-3) | 2.247.55 | 7.80 (3.3) | 3.55 | 3.11 (-13) |

255

The longer the lifetime of the hydrogen perturbation, the larger the change in hydrogen burden in the atmosphere. A larger change in hydrogen burden leads to a larger forcing and forcing per flux of hydrogen (as shown in Fig. 4b for CH_4, Fig. 4c for O_3, and Fig. 4d for strat. H_2O) and larger GWP100. Similarly, a smaller change in atmospheric hydrogen per hydrogen flux leads to smaller forcing and smaller GWP100 values. Although there is a spread in the GWP values of 4.1, the results are within the one sigma uncertainty range in the multi-model study by Sand et al. (2023) of 9.4 to 13.9, with the exception of nemo and maud that are just outside this range, both with a GWP100 of 14.2. One should note that these two sites have an extreme location relative to what can be expected in a future hydrogen economy. For the continental sites more relevant for a future hydrogen economy (usdrydep, munich, lowlatdep, epia) the GWP100 range from 10.2 to 11.9, slightly less than perturbing the total anthropogenic emissions (anthro1) of 12.5.

3.3 Does the chemical background matter?

In the future, the chemical composition of the atmosphere may be different than for present-day. As future emissions of chemically active components depend on technological developments and future societal evolution, different scenarios span possible pathways for emissions and concentrations of these reactive species.

Before looking at the sensitivity of the calculated GWP to the atmospheric chemical background, we will look at the hydrogen and methane budget in 2050. For all the SSP simulations we have used the same hydrogen emissions as in the present-day simulations (CNTR), so the changes in the hydrogen budgetburden are only due to changes in atmospheric production and loss of hydrogen. Table 4 shows how the hydrogen budget changes in the three different SSP steady state simulations for 2050, relative to the 2010 steady state conditions used in the present-day simulation.

The hydrogen burden (as well as surface concentration) decreases in SSP119 mainly due to a decrease in the atmospheric production of hydrogen (Table 4). As chemical degradation of methane in the atmosphere is a main route of hydrogen production (Ehhalt and Rohrer, 2009;Paulot et al., 2021) the reduction in methane in SSP119 (Table 2, Fig. 2) as well as anthropogenic emissions of non-methane VOCs (Fig. S1), lower the amount of hydrogen in the atmosphere. In the two other scenarios, the methane levels are higher (Table 2, Fig. 2) and hydrogen production and burden increases (Table 4). Note that we only change the atmospheric composition and do not change the climatic conditions in these simulations. As expected, the soil sink lifetime is similar in these simulations (Table 4) as the meteorology is the same.

Table 4: The hydrogen budget terms for present day (CNTR) and the change in these budget terms for the different SSPs relative to CNTR. The budget terms included are burden, surface concentration, atmospheric productions and the sink represented as lifetimes. The hydrogen emissions are set equal in all the simulations.

	H_2 burden	H_2 surface concentration	H_2 atmospheric production	H_2 atmospheric lifetime	H_2 soil sink lifetime	H_2 total lifetime
	[Tg]	[ppbv]	[Tg yr^{-1}]	[yrs]	[yrs]	[yrs]
CNTR	205	559	55.8	7.02	3.53	2.35
SSP119 – CNTR	-23.6	-63.9	-10.8	0.24	-0.01	0.02
SSP434 – CNTR	20.4	54.1	4.62	0.93	0.02	0.10
SSP585 – CNTR	29.5	78.9	9.85	0.53	0.02	0.07

The atmospheric lifetime of hydrogen, calculated as the atmospheric burden divided by the ~~chemistry~~chemical loss~~,~~ through OH (Eq. 1). depends on the chemical composition of the atmosphere. A larger concentration of methane will reduce the available OH, and the atmospheric lifetime of both methane and hydrogen will increase. In addition to methane, the NO_x to CO emission ratio is also an important factor controlling OH in the atmosphere (Dalsøren et al., 2016). In all the scenarios the atmospheric lifetime of hydrogen increases (Table 4). For SSP434, both the increased methane concentration and the lower NO_x to CO emission ratio (Fig. 2) push in the direction of less OH and a longer hydrogen atmospheric lifetime. This is the scenario where the hydrogen atmospheric lifetime increased the most by 0.9 years. In SSP119, the methane concentration is lower than for present day, contributing to a shorter hydrogen atmospheric lifetime, while the NO_x to CO emission ratio (Fig. 2) pushes in the direction of a longer atmospheric lifetime. The resulting change in the hydrogen atmospheric lifetime is an increase by 0.2 years in SSP119 in 2050 compared to the present-day simulations. For SSP585, the methane and NO_x to CO emission ratios change relative to present day also act in different directions with respect to OH and atmospheric lifetime of hydrogen. The hydrogen atmospheric lifetime increases by 0.5 years in this scenario in 2050 relative to present day. There are no scenarios with reduced methane concentration and higher NO_x to CO emission ratios where both would have pushed in the direction of a shorter hydrogen atmospheric lifetime. As soil sink is the dominant loss term for hydrogen, the total lifetime change is smaller than the change in atmospheric lifetime, and the largest increase in total lifetime is for SSP434 with 0.1 years.

Table 5 shows the methane budget terms for present-day and the respective changes in the three SSPs. The change in the methane lifetime due to OH is similar to the change in the hydrogen atmospheric lifetime. As the total methane lifetime is dominated by the OH loss, the total lifetime of methane increases by 0.9 years in SSP434 relative to present day.

Table 5: The methane budget terms for present-day (CNTR) and the change in these budget terms for the different SSPs relative to CNTR. For the total lifetime a soil sink lifetime of 160 years and a stratospheric lifetime (excluding OH loss) of 240 years is assumed as in Sand et al. (2023).

	CH_4 burden [Tg]	CH_4 surface concentration [ppbv]	CH_4 lifetime due to OH (whole atmosphere) [yrs]	Total CH_4 lifetime [yrs]	Feedback factor	Perturbation lifetime
CNTR	4975	1813	7.38	6.85	1.46	10.04
SSP119 – CNTR	-1059	-386	0.29	0.25	0.05	0.72
SSP434 – CNTR	1129	410	1.05	0.90	0.25	3.24
SSP585 – CNTR	1738	633	0.61	0.52	0.21	2.31

310

The H_2 GWP100 for the different atmospheric composition sensitivity tests are shown in Fig. 3, ranging from 12.9 to 13.5 compared to 12.6 (anthro10) for 2010 atmospheric composition. For the geographical location sensitivity test (section 3.2), the H_2 GWP100 differed due to differences in the perturbation lifetimes. For the sensitivity tests with different chemical backgrounds, the perturbation lifetimes are similar to present day conditions (anthro10) (Table 3) and the changes in surface concentration of hydrogen per hydrogen flux are similar to anthro10 (Fig. 3a).

315

For the direct contribution to methane ERF per hydrogen flux (the area not hatched in Fig. 4b) the contribution is very similar for the different SSPs. For the methane induced changes (hatched part of the bars), there are larger differences, with larger contribution in SSP585 and SSP434 compared to present day (anthro10) and SSP119. The methane induced relative contribution to the GWP100 is hence larger in SSP585 and SSP434 compared to SSP119 (Table S5). The methane induced changes for methane ERF per hydrogen flux is estimated based on the methane feedback factor. The methane feedback factor increases by 0.25 and 0.21 in SSP434 and SSP585 respectively, while in SSP119 the feedback factor only increases by 0.05 compared to present-day (Table 5).

320

For ozone ERF per hydrogen flux, the direct (unhatched part in Fig. 4c) and the total (entire bar in Fig. 4c) contribution from hydrogen perturbation is larger in SSP119 compared to the two other SSPs. Ozone contributes 42% of the total GWP100 in SSP119 while in the two other scenarios it contributes 37% (Table S6). The changes in methane ERF and ozone ERF per flux are compensating, which result in very similar GWP100 values for the different scenarios (Fig. 3) ranging from 12.9 in SSP119 to 13.5 in SSP585. The GWP100 increases by 3.0% to 7.8% when chemical background from three different SSPs for the year 2050 is used compared to using a present-day atmospheric composition in the simulations (Fig. S2).

325

Based on the methane perturbation experiments, the GWP100 of methane can also be calculated, as was done in the multi-model study by Sand et al. (2023). The methane chemical feedback factor increased from a present-day value of 1.46 to 1.71 in SSP434, which is a main reason why the methane GWP100 is largest in this scenario (Fig. 5). The ozone contribution to

330

the methane GWP100 is largest in SSP119, while the methane contribution to the GWP100 is smaller in SSP119 compared to the two other SSPs. Calculated CH_4 GWP100 increases by 6 to 13% in the SSPs for year 2050 relative to the present-day atmospheric composition. The GWP100 values of 28.6 to 30.5 and 27.0 for present day conditions (Table S8, Fig. 5) are however well within the uncertainty range of 19 to 35 from IPCC AR6 if the uncertainty in the AGWP for CO_2 is excluded (Forster et al., 2021;Smith et al., 2021).
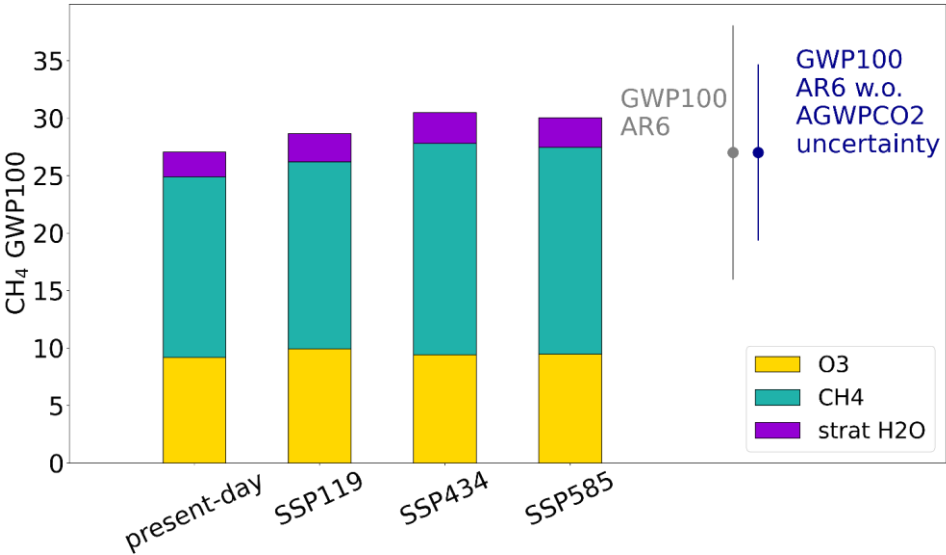
Figure 5: GWP100 for methane calculated based on simulations with present-day and three SSPs atmospheric composition for 2050 with individual contributions from methane (green), ozone (yellow), and stratospheric water vapor (purple). The IPCC AR6 uncertainty range is the 5-95% range for GWP100 non-fossil fuel methane (Forster et al., 2021) and the range excluding uncertainties in AGWP for CO_2 (Smith et al., 2021). The GWP100 values are presented in Table S7.

4. Discussion

~~In this study, we have used one of the models included in the multi-model study by Sand et al. (2023) to investigate the sensitivity of the H_2 GWP100 on how the hydrogen emission perturbation is added in the model simulations. In Sand et al. (2023) the main simulations were concentration driven, but perturbing hydrogen emissions resulted in similar GWP values as perturbing the concentration within one model (Sand et al., 2023).~~

In this study, we have used a chemical transport model to investigate the sensitivity of the H_2 GWP100 on how the hydrogen emission perturbation is added in the model simulations.

350 We find that GWP100 is independent of the size of the emission perturbation in the range of 0.1 to 100 Tg yr^{-1} explored in this sensitivity study. A linear response with respect to the size of the perturbation was also found by Derwent (2023) using a two-dimensional tropospheric chemistry-transport model. Derwent (2023) investigated also the latitudinal dependence of the emission pulse on the calculated GWP. In the two-dimensional model, without longitudinal dimension, Derwent (2023) found that the GWP depended on latitude, with the largest GWP values in the southernmost latitude band and the smallest

355 GWP values in the northernmost latitude band. This is also what we find for the Arctic (zep) and Antarctic (maud) emission locations with H_2 GWP100 of 11.7 and 14.2 respectively. The reason for the north-south gradient in the GWP is that the magnitude of the sink differs between the hemisphere due to different distribution of land and ocean areas (Derwent, 2023). However, with a three-dimensional model, we do find dependencies on the longitudinal distribution as well. We have carefully selected seven point locations and we find the distance to soil-sink active areas to be important for the calculated

360 GWP.

The reason for the different GWP values in the geographical sensitivity tests can be explained by differences in the hydrogen feedback factor.perturbation lifetime. For the sites nemo and maud, the feedback factorperturbation lifetime is larger than 1.enhanced relative to the lifetime of hydrogen in the control simulation. For sites close to areas where hydrogen can be taken up by the soil, the feedback factorperturbation lifetime is lessshorter than 1the hydrogen lifetime. This is because the

365 soil sink is enhanced when emissions are close to the soil sink active areas relative to the total soil sink. The feedback factor is therefore less than 1. In In Sand et al. (2023) the feedback factors are the perturbation lifetime relative to the background lifetime is slightly less than one, and ranges from 0.95 to 1.0. These simulations were mostly concentration driven and hydrogen concentration was enhanced by 10% globally. For the geographical sensitivity tests, the feedback factor range was much wider from 0.85 to 1.10, and hence a larger range in perturbation lifetime (was from 1.8 to 2.6 years) and GWP100,

370 25% shorter to 10% longer than the background lifetime. The GWP100 (10.2 to 14.2). The GWP100) values span the one standard deviation range from Sand et al. (2023), but note that some of the sites chosen are remote locations (in the Arctic, Antarctic, Southern Ocean) that are not relevant locations for future hydrogen economy. For continental sites more relevant for a future hydrogen economy, the GWP100 values are well within the one standard deviation range assessed in Sand et al. (2023).

375 The hydrogen economy is expected to grow, and in the future, the atmospheric composition might be different than that of the 2010 conditions used to calculate GWP100 in the multi-model study by Sand et al. (2023).. Therefore, we also investigated the sensitivity to the GWP100 by doing the emission perturbations on top of three different 2050 atmospheres based on SSP scenarios. The three different SSPs have different combinations of NO_x to CO emission ratios and methane levels that both influence the atmospheric lifetime of hydrogen. The atmospheric lifetime of both hydrogen and methane

380 increased in all the scenarios, and in SSP434 by as much as ~1 year. Also, the methane chemical feedback factor increased from 1.46 to 1.71 (17%) in SSP434. A feedback factor of 1.7 is larger than what is found for present day atmospheres where the methane feedback factor ~~ranges from 1.36 to 1.55 in Sand et al. (2023) and in other multi-model studies~~in multi-model studies ranges from 1.36 to 1.55 (Sand et al., 2023), 1.34 ± 0.06 (Holmes et al., 2013) and 1.30 ± 0.07 (Thornhill et al., 2020). Voulgarakis et al. (2013) also found an increase in the feedback factor from 1.24 for present day conditions to 1.50 in

385 2100 for a high methane low NO_x scenario that included changes in climatic factors in addition to the changes in atmospheric chemistry composition. A larger feedback factor will enhance the methane induced contribution to the GWP100 (hatched green part in Fig. 3). As methane lifetime is low in this model (Table 5) compared to assessed estimates 9.1 ± 0.9 years (Szopa et al., 2021), the resulting methane feedback factor and chemical response following a perturbation, may be different in a model with lower OH levels and longer methane lifetime.

390 From the methane perturbation experiments, the CH_4 GWP100 can also be calculated. The CH_4 GWP100 increased by 1.6 (6%) to 3.4 (13%) depending on the scenarios. These increases are driven by the increases in the perturbation lifetime of methane due to the change in the atmospheric composition of chemically reactive components in the scenarios. Note that changes in lightning emissions of NO_x, humidity, temperature and UV-radiation also alter the atmospheric oxidation capacity (Nicely et al., 2018;Dalsøren et al., 2016;Voulgarakis et al., 2013) but future changes in these are not included here. Liu et

395 al. (2024) investigated the future changes in the oxidation capacity in three global climate model simulations using two of the other SSPs. For a high mitigation scenario, with limited global warming, and reduced methane concentration (SSP126) the methane lifetime decreased by a range of 0.19 ~~to~~ 1.1 years due to increased OH concentration. For a low mitigation scenario with increased methane concentration and large temperature change (SSP370) the methane lifetime increased due to changes in the atmospheric composition partly masked by changes in climate, resulting in a total increase of 0.43 to 1.7 years

400 from 2015 to 2100. Note that the NO_x to CO anthropogenic emission ratios for 2050 are similar to the present-day ratio in these two scenarios. As noted above, the modelled methane lifetime is short and hence the OH level is high. Lower OH levels will enhance the lifetime of methane and the CH_4 GWP values but also impact the atmospheric chemistry involving ozone production. Further studies should investigate the role of OH levels on both H_2 and CH_4 GWP100 estimates.

For the H_2 GWP100, where the soil sink is the dominant control on the total lifetime, we find that the GWP100 values

405 increase slightly compared to the present-day values when atmospheric composition is changed. The soil sink uncertainty is the main contributor to the uncertainty in H_2 GWP100 (Sand et al., 2023). There are large knowledge gaps in our understanding and representation of soil sink in models (Paulot et al., 2021) and hence knowledge gaps in understanding historical, present-day and future changes in the largest term in the hydrogen budget (Ehhalt and Rohrer, 2009). There is indication of an increase in soil sink over the recent years in the Northern Hemisphere due to changes in soil moisture, soil

410 temperature and snow cover (Paulot et al., 2024). Future work should investigate potential changes in soil sink driven by climatic changes and assess how it will influence H_2 GWP100 values.

5. Conclusions

In this study we have used a chemistry transport model to investigate the sensitivity of the calculated H_2 GWP100 to the magnitude of the hydrogen emission perturbation, the location of the hydrogen emission perturbation as well as the chemical composition of the background atmosphere.

The H_2 GWP100 values are not dependent on the magnitude of the emission perturbation, with values ranging from 12.2 to 12.6 but ~~it depends~~are somewhat dependent on the location of the hydrogen perturbation in the model with values ranging from 10.2 to 14.2. The further away from soil sink active areas, the larger the GWP100 values. The values fall within the one standard deviation uncertainty range estimated in Sand et al. (2023) with the exception of the two most extreme locations, in the southern Pacific and in Antarctica, where the values are slightly larger. One should note that these two locations are not relevant sites for hydrogen usage in a future hydrogen economy. For other short-lived components, emission location matters for the radiative response (Berntsen et al., 2006) and GWP values are reported regionally (Myhre et al., 2013;Aamaas et al., 2016). The results here indicate that this is not necessary for hydrogen.

~~The H_2 GWP100 depends on the chemical composition of the atmosphere. In particular, the~~The methane levels and NO_x to CO emission ratio influence the oxidation capacity of the atmosphere and hence the lifetime of both methane and hydrogen. We have investigated how the H_2 GWP100 depends on the chemical composition of the atmosphere using SSP scenarios. In SSP585, where methane levels in 2050 are 35% above 2010 levels, the H_2 GWP100 is 13.5 and close to the upper range of the uncertainty range (+1 standard deviation) in Sand et al. (2023) and 7.8% larger than the H_2 GWP100 calculated here using present day atmospheric chemical composition. The atmospheric lifetime of hydrogen, as well as the methane lifetime, methane feedback factor and CH_4 GWP100 depend on the chemical composition of the atmosphere. For hydrogen, however, the dominant factor for the total lifetime is the soil sink. A better understanding of the soil sink processes and how the soil sink may be affected by climate change is needed to further investigate how H_2 GWP100 may change in the future.

In conclusion, the H_2 GWP100 is independent of the size of the emission perturbation, depends to some degree on the emission location (distance to soil sink active areas) and depends slightly on the chemical background atmosphere. Overall, these dependencies are small compared to the uncertainty in the H_2 GWP100 due to ~~process~~weaknesses in understanding of the processes controlling the hydrogen budget.

Code availability

~~The code to reproduce the figures in this manuscript: https://github.com/ciceroOslo/Hydrogen_GWP_sensitivity/tree/main~~

440 The code to reproduce the figures in this manuscript can be found at https://zenodo.org/records/14823343 (Skeie et al., 2025). The OsloCTM3 version used here are available at https://github.com/ciceroOslo/OsloCTM3/releases/tag/hydrogen-sensitivity-v1.

Data availability

The data needed to reproduce the figures in the manuscript:

445 https://github.com/ciceroOslo/Hydrogen_GWP_sensitivity/tree/main. The full dataset for the model results will be made available in the NIRD Research Data Archive upon publication.

The data needed to reproduce the figures in the manuscript can be found at https://zenodo.org/records/14823343 (Skeie et al., 2025). The full dataset for the model results is available in the NIRD Research Data Archive: https://doi.org/10.11582/2025.00008 (Skeie, 2025).

450 **Author contribution**

RBS wrote the paper with contributions from all co-authors. Marit S designed the geographical experiments, RBS designed the SSP experiments. RBS performed the OsloCTM3 simulations. All co-authors discussed the design and results.

Competing interests

GMAt least one of the (co-)authors is a member of the editorial board of Atmospheric Chemistry and Physics.

455 **Acknowledgements**

The work has received funding from the Norwegian Research Council (80%) and and six industrial partners (20%): Shell, Equinor, Statkraft, Linde, Gassco and Norwegian Shipowners' Associations (HYDROGEN, grants no. 320240) and the European Union's Horizon Europe research and innovation programme under grant agreement no. 101137582 (HYway). The OsloCTM3 simulations were performed on resources provided by Sigma2 - the National Infrastructure for High-Performance Computing and Data Storage in Norway (project account NN9188K), and data will be uploaded and shared through their services (project NS11106K and NS9188K) upon publication.).

References

Allen, M. R., Fuglestvedt, J. S., Shine, K. P., Reisinger, A., Pierrehumbert, R. T., and Forster, P. M.: New use of global warming potentials to compare cumulative and short-lived climate pollutants, Nature Climate Change, 6,773-776, 10.1038/nclimate2998, 2016.

Allen, M. R., Shine, K. P., Fuglestvedt, J. S., Millar, R. J., Cain, M., Frame, D. J., and Macey, A. H.: A solution to the misrepresentations of CO2-equivalent emissions of short-lived climate pollutants under ambitious mitigation, npj Climate and Atmospheric Science, 1,16, 10.1038/s41612-018-0026-8, 2018.

470 Berntsen, T., Fuglestvedt, J., Myhre, G., Stordal, F., and Berglen, T. F.: Abatement of greenhouse gases: Does location matter?, Clim. Change, 74,377-411, 2006.

Cain, M., Lynch, J., Allen, M. R., Fuglestvedt, J. S., Frame, D. J., and Macey, A. H.: Improved calculation of warming-equivalent emissions for short-lived climate pollutants, npj Climate and Atmospheric Science, 2,29, 10.1038/s41612-019-0086-4, 2019.

Dalsøren, S. B., Myhre, C. L., Myhre, G., Gomez-Pelaez, A. J., Søvde, O. A., Isaksen, I. S. A., Weiss, R. F., and Harth, C.
475 M.: Atmospheric methane evolution the last 40 years, Atmos. Chem. Phys., 16,3099-3126, 10.5194/acp-16-3099-2016, 2016.

Derwent, R. G., Collins, W. J., Johnson, C. E., and Stevenson, D. S.: Transient Behaviour of Tropospheric Ozone Precursors in a Global 3-D CTM and Their Indirect Greenhouse Effects, Clim. Change, 49,463-487, 10.1023/A:1010648913655, 2001.

Derwent, R. G., Stevenson, D. S., Utembe, S. R., Jenkin, M. E., Khan, A. H., and Shallcross, D. E.: Global modelling studies
480 of hydrogen and its isotopomers using STOCHEM-CRI: Likely radiative forcing consequences of a future hydrogen economy, Int. J. Hydrogen Energy, 45,9211-9221, https://doi.org/10.1016/j.ijhydene.2020.01.125, 2020.

Derwent, R. G.: Global warming potential (GWP) for hydrogen: Sensitivities, uncertainties and meta-analysis, Int. J. Hydrogen Energy, 48,8328-8341, https://doi.org/10.1016/j.ijhydene.2022.11.219, 2023.

DNV: Hydrogen Forecast to 2050 (https://www.dnv.com/focus-areas/hydrogen/forecast-to-2050/), 2022.
485 Ehhalt, D. H., and Rohrer, F.: The tropospheric cycle of H2: a critical review, Tellus B, 61,500-535, https://doi.org/10.1111/j.1600-0889.2009.00416.x, 2009.

Esquivel-Elizondo, S., Hormaza Mejia, A., Sun, T., Shrestha, E., Hamburg, S. P., and Ocko, I. B.: Wide range in estimates of hydrogen emissions from infrastructure, Frontiers in Energy Research, 11, 10.3389/fenrg.2023.1207208, 2023.

Etminan, M., Myhre, G., Highwood, E. J., and Shine, K. P.: Radiative forcing of carbon dioxide, methane, and nitrous oxide:
490 A significant revision of the methane radiative forcing, Geophys. Res. Lett., 43,12,614-612,623, 10.1002/2016GL071930, 2016.

Fesenfeld, L. P., Schmidt, T. S., and Schrode, A.: Climate policy for short- and long-lived pollutants, Nature Climate Change, 8,933-936, 10.1038/s41558-018-0328-1, 2018.

Field, R. A., and Derwent, R. G.: Global warming consequences of replacing natural gas with hydrogen in the domestic
495 energy sectors of future low-carbon economies in the United Kingdom and the United States of America, Int. J. Hydrogen Energy, 46,30190-30203, https://doi.org/10.1016/j.ijhydene.2021.06.120, 2021.

Forster, P., T. Storelvmo, K. Armour, W. Collins, J. L. Dufresne, D. Frame, D. J. Lunt, T. Mauritsen, M. D. Palmer, M. Watanabe, M. Wild, and Zhang, H.: The Earth's Energy Budget, Climate Feedbacks, and Climate Sensitivity, in: Climate Change 2021: The Physical Science Basis. Contribution of Working Group I to the Sixth Assessment Report of the
500 Intergovernmental Panel on Climate Change, edited by: Masson-Delmotte, V., P. Zhai, A. Pirani, S. L. Connors, C. Péan, S. Berger, N. Caud, Y. Chen, L. Goldfarb, M. I. Gomis, M. Huang, K. Leitzell, E. Lonnoy, J. B. R. Matthews, T. K. Maycock, T. Waterfield, O. Yelekçi, R. Yu, and Zhou, B., Cambridge University Press, Cambridge, United Kingdom and New York, NY, USA, 2021.

Gidden, M. J., Riahi, K., Smith, S. J., Fujimori, S., Luderer, G., Kriegler, E., van Vuuren, D. P., van den Berg, M., Feng, L.,
505 Klein, D., Calvin, K., Doelman, J. C., Frank, S., Fricko, O., Harmsen, M., Hasegawa, T., Havlik, P., Hilaire, J., Hoesly, R., Horing, J., Popp, A., Stehfest, E., and Takahashi, K.: Global emissions pathways under different socioeconomic scenarios for use in CMIP6: a dataset of harmonized emissions trajectories through the end of the century, Geosci. Model Dev., 12,1443-1475, 10.5194/gmd-12-1443-2019, 2019.

Hauglustaine, D., Paulot, F., Collins, W., Derwent, R., Sand, M., and Boucher, O.: Climate benefit of a future hydrogen
510 economy, Communications Earth & Environment, 3,295, 10.1038/s43247-022-00626-z, 2022.

Hoesly, R. M., Smith, S. J., Feng, L., Klimont, Z., Janssens-Maenhout, G., Pitkanen, T., Seibert, J. J., Vu, L., Andres, R. J., Bolt, R. M., Bond, T. C., Dawidowski, L., Kholod, N., Kurokawa, J. I., Li, M., Liu, L., Lu, Z., Moura, M. C. P., O'Rourke, P. R., and Zhang, Q.: Historical (1750–2014) anthropogenic emissions of reactive gases and aerosols from the Community Emissions Data System (CEDS), Geosci. Model Dev., 11,369-408, 10.5194/gmd-11-369-2018, 2018.

515 Holmes, C. D., Prather, M. J., Søvde, O. A., and Myhre, G.: Future methane, hydroxyl, and their uncertainties: key climate and emission parameters for future predictions, Atmos. Chem. Phys., 13,285-302, 10.5194/acp-13-285-2013, 2013.

HydrogenCouncil: Hydrogen   Insights   May   2023   Hydrogen   Council,   McKinsey   &   Company, https://hydrogencouncil.com/en/hydrogen-insights-2023/ 2023.

IEA: Global Hydrogen Review 2023 https://www.iea.org/reports/global-hydrogen-review-2023, IEA, Paris, 2023.

520 Liu, M., Song, Y., Matsui, H., Shang, F., Kang, L., Cai, X., Zhang, H., and Zhu, T.: Enhanced atmospheric oxidation toward carbon neutrality reduces methane's climate forcing, Nature Communications, 15,3148, 10.1038/s41467-024-47436-9, 2024.

Lynch, J., Cain, M., Pierrehumbert, R., and Allen, M.: Demonstrating GWP*: a means of reporting warming-equivalent emissions that captures the contrasting impacts of short- and long-lived climate pollutants, Environ. Res. Let., 15,044023, 10.1088/1748-9326/ab6d7e, 2020.

525 Meinshausen, M., Nicholls, Z. R. J., Lewis, J., Gidden, M. J., Vogel, E., Freund, M., Beyerle, U., Gessner, C., Nauels, A., Bauer, N., Canadell, J. G., Daniel, J. S., John, A., Krummel, P. B., Luderer, G., Meinshausen, N., Montzka, S. A., Rayner, P. J., Reimann, S., Smith, S. J., van den Berg, M., Velders, G. J. M., Vollmer, M. K., and Wang, R. H. J.: The shared socio-economic pathway (SSP) greenhouse gas concentrations and their extensions to 2500, Geosci. Model Dev., 13,3571-3605, 10.5194/gmd-13-3571-2020, 2020.

530 Monks, P. S., Archibald, A. T., Colette, A., Cooper, O., Coyle, M., Derwent, R., Fowler, D., Granier, C., Law, K. S., Mills, G. E., Stevenson, D. S., Tarasova, O., Thouret, V., von Schneidemesser, E., Sommariva, R., Wild, O., and Williams, M. L.: Tropospheric ozone and its precursors from the urban to the global scale from air quality to short-lived climate forcer, Atmos. Chem. Phys., 15,8889-8973, 10.5194/acp-15-8889-2015, 2015.

Myhre, G., Nilsen, J. S., Gulstad, L., Shine, K. P., Rognerud, B., and Isaksen, I. S. A.: Radiative forcing due to stratospheric

535 water vapour from CH4 oxidation, Geophys. Res. Lett., 34,L01807, 10.1029/2006gl027472, 2007.

Myhre, G., D. Shindell, F.-M. Bréon, W. Collins, J. Fuglestvedt, J. Huang, D. Koch, J.-F. Lamarque, D. Lee, B. Mendoza, T. Nakajima, A. Robock, G. Stephens, T. Takemura, and Zhang, H.: Anthropogenic and Natural Radiative Forcing, in: Climate Change 2013: The Physical Science Basis. Contribution of Working Group I to the Fifth Assessment Report of the Intergovernmental Panel on Climate Change edited by: Stocker, T. F., D. Qin, G.-K. Plattner, M. Tignor, S.K. Allen, J.

540 Boschung, A. Nauels, Y. Xia, V. Bex, and Midgley, P. M., Cambridge University Press, Cambridge, United Kingdom and New York, NY, USA, 2013.

Nicely, J. M., Canty, T. P., Manyin, M., Oman, L. D., Salawitch, R. J., Steenrod, S. D., Strahan, S. E., and Strode, S. A.: Changes in Global Tropospheric OH Expected as a Result of Climate Change Over the Last Several Decades, J. Geophys. Res., 123,10,774-710,795, https://doi.org/10.1029/2018JD028388, 2018.

545 Paulot, F., Paynter, D., Naik, V., Malyshev, S., Menzel, R., and Horowitz, L. W.: Global modeling of hydrogen using GFDL-AM4.1: Sensitivity of soil removal and radiative forcing, Int. J. Hydrogen Energy, 46,13446-13460, https://doi.org/10.1016/j.ijhydene.2021.01.088, 2021.

Paulot, F., Pétron, G., Crotwell, A. M., and Bertagni, M. B.: Reanalysis of NOAA H2 observations: implications for the H2 budget, Atmos. Chem. Phys., 24,4217-4229, 10.5194/acp-24-4217-2024, 2024.

550 Prather, M. J.: Lifetimes of atmospheric species: Integrating environmental impacts, Geophys. Res. Lett., 29,20-21-20-23, https://doi.org/10.1029/2002GL016299, 2002.

Prather, M. J.: An Environmental Experiment with H₂?, Science, 302,581-582, doi:10.1126/science.1091060, 2003.

Prather, M. J.: Lifetimes and time scales in atmospheric chemistry, Philosophical Transactions of the Royal Society A: Mathematical, Physical and Engineering Sciences, 365,1705-1726, doi:10.1098/rsta.2007.2040, 2007.

555 Price, H., Jaeglé, L., Rice, A., Quay, P., Novelli, P. C., and Gammon, R.: Global budget of molecular hydrogen and its deuterium content: Constraints from ground station, cruise, and aircraft observations, J. Geophys. Res., 112, https://doi.org/10.1029/2006JD008152, 2007.

Sand, M., Skeie, R. B., Sandstad, M., Krishnan, S., Myhre, G., Bryant, H., Derwent, R., Hauglustaine, D., Paulot, F., Prather, M., and Stevenson, D.: A multi-model assessment of the Global Warming Potential of hydrogen, Communications Earth &

560 Environment, 4,203, 10.1038/s43247-023-00857-8, 2023.

Sanderson, M. G., Collins, W. J., Derwent, R. G., and Johnson, C. E.: Simulation of Global Hydrogen Levels Using a Lagrangian Three-Dimensional Model, Journal of Atmospheric Chemistry, 46,15-28, 10.1023/A:1024824223232, 2003.

Saunois, M., Stavert, A. R., Poulter, B., Bousquet, P., Canadell, J. G., Jackson, R. B., Raymond, P. A., Dlugokencky, E. J., Houweling, S., Patra, P. K., Ciais, P., Arora, V. K., Bastviken, D., Bergamaschi, P., Blake, D. R., Brailsford, G., Bruhwiler,

565 L., Carlson, K. M., Carrol, M., Castaldi, S., Chandra, N., Crevoisier, C., Crill, P. M., Covey, K., Curry, C. L., Etiope, G., Frankenberg, C., Gedney, N., Hegglin, M. I., Höglund-Isaksson, L., Hugelius, G., Ishizawa, M., Ito, A., Janssens-Maenhout, G., Jensen, K. M., Joos, F., Kleinen, T., Krummel, P. B., Langenfelds, R. L., Laruelle, G. G., Liu, L., Machida, T., Maksyutov, S., McDonald, K. C., McNorton, J., Miller, P. A., Melton, J. R., Morino, I., Müller, J., Murguia-Flores, F., Naik, V., Niwa, Y., Noce, S., O'Doherty, S., Parker, R. J., Peng, C., Peng, S., Peters, G. P., Prigent, C., Prinn, R., Ramonet, M.,
570 Regnier, P., Riley, W. J., Rosentreter, J. A., Segers, A., Simpson, I. J., Shi, H., Smith, S. J., Steele, L. P., Thornton, B. F., Tian, H., Tohjima, Y., Tubiello, F. N., Tsuruta, A., Viovy, N., Voulgarakis, A., Weber, T. S., van Weele, M., van der Werf, G. R., Weiss, R. F., Worthy, D., Wunch, D., Yin, Y., Yoshida, Y., Zhang, W., Zhang, Z., Zhao, Y., Zheng, B., Zhu, Q., Zhu, Q., and Zhuang, Q.: The Global Methane Budget 2000–2017, Earth Syst. Sci. Data, 12,1561-1623, 10.5194/essd-12-1561-2020, 2020.
575 Shindell, D., Borgford-Parnell, N., Brauer, M., Haines, A., Kuylenstierna, J. C. I., Leonard, S. A., Ramanathan, V., Ravishankara, A., Amann, M., and Srivastava, L.: A climate policy pathway for near- and long-term benefits, Science, 356,493-494, 10.1126/science.aak9521, 2017.
Skeie, R. B., Myhre, G., Hodnebrog, Ø., Cameron-Smith, P. J., Deushi, M., Hegglin, M. I., Horowitz, L. W., Kramer, R. J., Michou, M., Mills, M. J., Olivié, D. J. L., Connor, F. M. O., Paynter, D., Samset, B. H., Sellar, A., Shindell, D., Takemura,
580 T., Tilmes, S., and Wu, T.: Historical total ozone radiative forcing derived from CMIP6 simulations, npj Climate and Atmospheric Science, 3,32, 10.1038/s41612-020-00131-0, 2020.
Skeie, R. B., Hodnebrog, Ø., and Myhre, G.: Trends in atmospheric methane concentrations since 1990 were driven and modified by anthropogenic emissions, Communications Earth & Environment, 4,317, 10.1038/s43247-023-00969-1, 2023.
Skeie, R. B. OsloCTM3 results for hydrogen emission perturbation sensitivity study,https://doi.org/10.11582/2025.00008
585 (2025).
Skeie, R. B., Sandstad, M., and mariasand. ciceroOslo/Hydrogen_GWP_sensitivity: v1.0.1,https://doi.org/10.5281/zenodo.14823343 (2025).
Smith, C., Z.R.J. Nicholls, K. Armour, W. Collins, P. Forster, M. Meinshausen, M.D. Palmer, and Watanabe, M.: The Earth's Energy Budget, Climate Feedbacks, and Climate Sensitivity Supplementary Material, in: Climate Change 2021: The
590 Physical Science Basis. Contribution of Working Group I to the Sixth Assessment Report of the Intergovernmental Panel on Climate Change, edited by: Masson-Delmotte, V., P. Zhai, A. Pirani, S.L. Connors, C. Péan, S. Berger, N. Caud, Y. Chen, L. Goldfarb, M.I. Gomis, M. Huang, K. Leitzell, E. Lonnoy, J.B.R. Matthews, T.K. Maycock, T. Waterfield, O. Yelekçi, R. Yu, and Zhou, B., Available from https://www.ipcc.ch/. 2021.
Szopa, S., V. Naik, B. Adhikary, P. Artaxo, T. Berntsen, W. D. Collins, S. Fuzzi, L. Gallardo, A. Kiendler Scharr, Z.
595 Klimont, H. Liao, N. Unger, and Zanis, P.: Short-Lived Climate Forcers, in: Climate Change 2021: The Physical Science Basis. Contribution of Working Group I to the Sixth Assessment Report of the Intergovernmental Panel on Climate Change, edited by: Masson-Delmotte, V., P. Zhai, A. Pirani, S. L. Connors, C. Péan, S. Berger, N. Caud, Y. Chen, L. Goldfarb, M. I. Gomis, M. Huang, K. Leitzell, E. Lonnoy, J. B. R. Matthews, T. K. Maycock, T. Waterfield, O. Yelekçi, R. Yu, and Zhou, B., Cambridge University Press, Cambridge, United Kingdom and New York, NY, USA 2021.
600 Søvde, O. A., Prather, M. J., Isaksen, I. S. A., Berntsen, T. K., Stordal, F., Zhu, X., Holmes, C. D., and Hsu, J.: The chemical transport model Oslo CTM3, Geosci. Model Dev., 5,1441-1469, 10.5194/gmd-5-1441-2012, 2012.
Thornhill, G. D., Collins, W. J., Kramer, R. J., Olivié, D., O'Connor, F., Abraham, N. L., Bauer, S. E., Deushi, M., Emmons, L., Forster, P., Horowitz, L., Johnson, B., Keeble, J., Lamarque, J. F., Michou, M., Mills, M., Mulcahy, J., Myhre, G., Nabat, P., Naik, V., Oshima, N., Schulz, M., Smith, C., Takemura, T., Tilmes, S., Wu, T., Zeng, G., and Zhang, J.: Effective
605 Radiative forcing from emissions of reactive gases and aerosols – a multimodel comparison, Atmos. Chem. Phys. Discuss., 2020,1-29, 10.5194/acp-2019-1205, 2020.
van der Werf, G. R., Randerson, J. T., Giglio, L., van Leeuwen, T. T., Chen, Y., Rogers, B. M., Mu, M., van Marle, M. J. E., Morton, D. C., Collatz, G. J., Yokelson, R. J., and Kasibhatla, P. S.: Global fire emissions estimates during 1997–2016, Earth Syst. Sci. Data, 9,697-720, 10.5194/essd-9-697-2017, 2017.
610 van Ruijven, B., Lamarque, J.-F., van Vuuren, D. P., Kram, T., and Eerens, H.: Emission scenarios for a global hydrogen economy and the consequences for global air pollution, Global Environmental Change, 21,983-994, https://doi.org/10.1016/j.gloenvcha.2011.03.013, 2011.
Voulgarakis, A., Naik, V., Lamarque, J. F., Shindell, D. T., Young, P. J., Prather, M. J., Wild, O., Field, R. D., Bergmann, D., Cameron-Smith, P., Cionni, I., Collins, W. J., Dalsøren, S. B., Doherty, R. M., Eyring, V., Faluvegi, G., Folberth, G. A.,

615   Horowitz, L. W., Josse, B., MacKenzie, I. A., Nagashima, T., Plummer, D. A., Righi, M., Rumbold, S. T., Stevenson, D. S., Strode, S. A., Sudo, K., Szopa, S., and Zeng, G.: Analysis of present day and future OH and methane lifetime in the ACCMIP simulations, Atmos. Chem. Phys., 13,2563-2587, 10.5194/acp-13-2563-2013, 2013.

Warwick, N. J., Archibald, A. T., Griffiths, P. T., Keeble, J., O'Connor, F. M., Pyle, J. A., and Shine, K. P.: Atmospheric composition and climate impacts of a future hydrogen economy, Atmos. Chem. Phys., 23,13451-13467, 10.5194/acp-23-
620   13451-2023, 2023.

Xiao, X., Prinn, R. G., Simmonds, P. G., Steele, L. P., Novelli, P. C., Huang, J., Langenfelds, R. L., O'Doherty, S., Krummel, P. B., Fraser, P. J., Porter, L. W., Weiss, R. F., Salameh, P., and Wang, R. H. J.: Optimal estimation of the soil uptake rate of molecular hydrogen from the Advanced Global Atmospheric Gases Experiment and other measurements, J. Geophys. Res., 112, https://doi.org/10.1029/2006JD007241, 2007.

625   Aamaas, B., Berntsen, T. K., Fuglestvedt, J. S., Shine, K. P., and Bellouin, N.: Regional emission metrics for short-lived climate forcers from multiple models, Atmos. Chem. Phys., 16,7451-7468, 10.5194/acp-16-7451-2016, 2016.